Quantitative Droplets for DNA Sequence Printing with a Low-voltage Logic Circuit, High-power Driver, and Micro-electromechanical Technology

Chih-Wei Peng,[1] Chen-Chia Chou,[2] Zhen-Xi Chen,[3] Jian-Chiun Liou[1]*

[1]School of Biomedical Engineering, Taipei Medical University, Taipei 11031, Taiwan
[2]Department of Mechanical Engineering, National Taiwan University of Science and Technology, Taipei, Taiwan
[3]Institute of Biophotonics, National Yang Ming Chiao Tung University, Taipei, Taiwan

In this study, inkjet printing was used to produce quantitative droplets of a DNA sequence using a novel, high-density, high-resolution nano-ink inkjet chip. It contains thousands of tiny orifices like very tiny volcano-shaped nozzles. This technology was used to design high-speed, high-voltage drive circuit systems. This chip integrates digital circuits, an optoelectronic thin-film process, and micro-electromechanical process technology on a single monolithic chip. The entire chip is a very large digital circuit that controls more than 1000 nano-ink nozzles. The circuit design simulates and uses a 0.18 µm line width high-voltage process to drive an array of micro-electromechanical elements. It can drive 432 nozzles very quickly within 85 µs. According to this specification, the high-precision nano-inkjet print head was extended to drive 1296 nozzles in a sequential manner. It can complete dynamic tracking measurements and analyze a low trajectory of inkjet liquid. In research and development in the field of DNA detection and medical electronics, the developed DNA spray array can be quantitatively distributed on a glass slide. This technology can be extended to high-speed, high-density nozzles and micro-liquid spray applications.

1. Introduction

In this study, we introduce how to eject nano-droplets in gene chip microarray technology. Traditional genetic testing needs to detect genes of interest one by one. Although this method can successfully produce results, it needs to be conducted using well-known target genes. The human genome has more than 20000 genes that face new drugs. The detection of unknown diseases requires guessing possible target genes before research begins. For example, guessing errors may result in an inability to find related genes, and so detection is very inefficient. In addition, traditional array genetic test equipment uses robotic arms. A module operates a micropipette and repeatedly moves between different reagents and sample containers to complete the detection steps. The process is quite time-consuming. Therefore, the carpet

---

detection method of a gene chip has many comparative advantages, and it is also the fastest growing type of biochip. By DNA replication, thousands or tens of thousands of nucleic acids can be probed, and this nucleic acid probe is enough to represent a certain special gene sequence. Nucleic acid probes are implanted into squares of ten thousands of micrometers on a chip. The nucleic acid probe is hybridized with the nucleic acid fragment to be detected, and owing to the concept of base conjugate complementarity in nucleic acids, if the nucleic acid fragment to be detected is complementary to the nucleic acid probe sequence, it will bond with the wafer. Finally, nucleic acid fragments that do not successfully bond are rinsed off with a wash solution, and the luminescence image of the biochip is displayed through a laser scanner. The degree of luminescence of the fluorescent dye on the nucleic acid probe can be used to determine the expression level of a specific gene. The nucleic acid probe knows the sequence of the successfully joined nucleic acid fragments, thus providing a large amount of gene sequence information.[1–8]

Designed and manufactured nano-ink jet print heads can be applied to current nucleic acid sequence [coronavirus disease 2019 (COVID-19) single RNA] detection technology. The whole world is on edge due to the outbreak of pneumonia. In addition to preventing the spread of epidemics and developing the best treatment methods, since the initial symptoms are similar to those of a common cold, the most important thing is to determine in the beginning how to confirm whether a suspected infection is a new type of coronavirus. Viral (e.g., COVID-19) infections require subsequent isolation and treatment. Fortunately, with advances in nucleic acid sequencing and molecular detection technology, when scientists isolate and purify virus particles for the first time, they can obtain viral RNA after purification using next-generation sequencing (NGS) technology. After the complete nucleic acid sequence is obtained (a single COVID-19 RNA is about 30 kb), the open reading frame of its gene can be compared on the basis of sequence data. With these data, the fastest method is to use quantitative polymerase chain reaction (qPCR) to detect the presence of viral nucleic acids, and real-time PCR can be used for DNA and RNA, which is why test reagents are quickly developed after an epidemic breaks out. A specific primer set can be designed on the basis of the largest difference between the nucleic acid sequence of the virus and the host genome sequence and the region where COVID-19 differs from other coronavirus sequences. Specific fluorescent primer probes can be used to perform qPCR with these three primers to specifically detect whether COVID-19 is present in a specimen; if it is combined with viral nucleic acids after purification and quantification by cesium chloride gradient centrifugation, detection can be achieved, and the amount of virus particles contained in the body can be determined.

To design and manufacture nano-ink inkjet print heads combined with lab-on-a-chip technology, a photoresist is coated onto a glass substrate, and then lithographic process technology is used to obtain a punch microchannel template, into which polydimethylsiloxane (PDMS) is poured, filling the mold. After curing, the template is removed, and the surface is modified and bonded onto a glass substrate. The laboratory chip is a one-piece multi-functional chip that uses microfluidic channels to construct various functional components, miniaturizing multiple steps such as sample pretreatment, mixing reactions, heating reactions, separation, detection, and culturing, which are all concentrated on the chip. Detection is completed by adding various functions to drive the sample or reagent to move to each component of the

microchannel. Additional functions include applying a voltage to generate electro-osmotic flow, using micro-pumps or centrifugal force, and so forth to conduct various traditional biological tests in the chemical laboratory. The advantage of the microfluidic chip is that it can reduce the reaction volume, the number of samples and amounts of expensive reagents, and cost, and can accurately handle a small volume of liquid; it is easy to manipulate, mix, move, heat, and cool a fluid on one chip. Several microfluidic channels can be constructed to achieve simultaneous detection. The microfluidic channels are mainly made of materials such as single-crystal silicon, glass, quartz, and high-molecular-weight polymer materials, such as PDMS and polyisoprene, which are the mainstream because they are easy to process, rich in variety, low in price, exhibit good light transmittance, and are convenient for optical detection. Wafers are produced using the replica molding method, which requires pre-made templates. Templates are generally made by lithographic process technology. They are divided into etched templates and negative photoresist molded templates. Etched templates are generally made with silicon wafers as substrates. A negative photoresist molding template is used to coat the negative photoresist onto a glass or silicon substrate, and the runner of the convex mold is left after lithography. A liquid polymer (such as PDMS) is evenly poured onto the template, and after curing, the template is removed to obtain the cured polymer. At this time, the microstructure on the template is also transferred to the surface of the polymer, and the surfaces of the polymer and glass are modified. Post-quality bonding results in a microfluidic wafer.

With continuous in-depth research into biochip technology, compared with traditional genetic tests using about ten genes at a time, the number of genetic chip tests can be increased by a thousand-fold, and the sequencing of the human genome, which originally cost US$10 billion, can now be completed for US$1000. In the medical field in the future, microfluidic chips can be used for genetic testing, drug screening, rapid disease diagnosis, food safety, and so forth, to achieve convenient and rapid detection results and bring huge changes to human lives. Next, we introduce and analyze the research phase of the design and manufacturing of nano-inkjet print heads.

2.   Materials and Methods

In this research, we extend inkjet printing technology to DNA droplet inkjet printing. The key component of this printing system is the printing of wafers. The design and manufacturing of jet-printed wafers are key factors that affect the size and volume of the droplets. Special digital chips are used for DNA in smart medical specimens and DNA sequence printing. Gene spray sequencing system technology is accurately and quantitatively implemented on a glass slide, and the cavity of the addressing spray liquid crystal structure is selected, that is, a large array is used. The principle of smart inkjet technology is to place a DNA solution on the sequenced genome to re-sequence the glass slide, and then perform DNA sequencing of each pattern. The advantage of quantitative droplets is the rapid and quantitative control of the droplets. The special large-array digital chip is designed to generate hot bubbles and droplets; the chip produces bubbles with considerable thrust in a very short time and pushes out the liquid. In a very short time, nucleation of the bubbles is complete, and pressure is generated to push the

liquid droplets out of the cavity to form micro-droplets containing genes. The DNA sequence, complementary (c) DNA sequence, RNA, and RNA sequence in the sample undergo special digital chip spray sequencing, which is designed as a smart medical application to integrate high-voltage, high-power signals using semiconductor complementary metal oxide semiconductor (CMOS) component technology. Output drive array and low-voltage high-speed signal semiconductor CMOS logic technology produce hot bubbles and droplets. This drive system technology accurately processes the level of logic signals. In bubble jet technology, heating electrodes are arranged on the tube wall at the position of the inkjet head, and a selected heating element is heated by electronic pulses to make the liquid jet head produce droplets.[9–15] In the design of semiconductors, high-speed, high-voltage components are generated and controlled by large arrays of micro-electromechanical components. When the pulse is heated in an instant, the heat generates bubbles, and the generated bubbles create pressure causing ink droplets to regenerate. After the contents of the heating chamber are ejected through the inkjet head, the printing liquid droplets are sprayed onto the surface of a glass substrate. The size of each droplet on the surface of the glass substrate depends on the power control of the MEMS heating device. The control system integrates a logical high-speed pulse timing CMOS control circuit, which simultaneously has high-current and high-voltage drive components and can be combined with MEMS micro-structure design liquid jet actuator components for wafer batch processing.[16–25]

2.1 Nano-ink spray droplet micro-electromechanical chip manufacturing integrated with process controlling monitors

The double diffusion to the oxide-poly-oxide (DD-OPO) structure of the low-resistance wafer is expected to result in a highly reliable driver. The specific nano-ink spray droplet MEMS chip manufacturing process is described as follows.

1. The threshold voltage (V_{TH}) must be above 1.5 V, because the breakdown voltage of the driver is significantly lower above the V_{TH} than below the V_{TH}, and a higher V_{TH} can ensure that the OFF driver has a greater breakdown voltage below the V_{TH}. Note that the method of increasing the V_{TH} by ion implantation is not appropriate, because it will cause the n+/p junction to break easily. The low-resistance wafer process is a better choice, but the process parameters must be determined and verified.

2. The breakdown voltage (V_{BK}) must be above 11 V (@ $V_G > V_{TH}$). This means that when voltage gain (V_G) > V_{TH}, the driver (non-test key) can have a V_{BK} above 11 V. The current MOSFET test key with $W = 20$ mm and $L = 4$ mm is $V_{BK} = 17$ V @ $V_G = 0$ or $V_{BK} = 11$ V @ $V_G > V_{TH}$, but the driver's V_{BK} @ $V_G > V_{TH}$ is only 5–7 V.

3. The test key must be complete.

In the development of new processes and new products, the test key or process controlling monitors (PCMs) are more important than the actual layout. PCM MOSFET (Table 1), test key layout (Fig. 1), and PCM design must meet the following process reality as shown in Table 2.

The test key or PCM design must meet the process conditions as shown in Table 1, and those for nano-inkjet process control monitors (PCMs) are given in Table 2.

Table 1
PCM and Test-key of MOSFET.

PCM		
Codename	Content	Eligibility criteria
FIO	Field isolation	Open and leakage
PPO	Poly-Si etching off	Open, on LOCOS step
PSO	Poly-Si on substrate capacitor	Open and leakage
PSR	Poly-Si sheet resistance	—
PMC	Poly-Si to metal contact	Resistance < some value
MNC	Metal to n+ implant contact	—
MPC	Metal to p+ implant contact	Resistance
M1O	Metal to metal etching off	Open
M1R	Metal resistance	—
NF4	N+ implant field spacing 4 mm	Open
NP4	N+ implant	100 square
MSI	Metal to substrate isolation	Open
MPI	Metal to poly isolation	Open, on poly/LOCOS step
Test-key MOSFET		
Codename	Content	Eligibility criteria
FND	N+/P diode, field surrounding	Leakage, V_{BK}
PND	N+/P diode, n+ poly surrounding	—
FIT	Field transistor	$V_{TH} > 12$ V
MT20	$W = 20$ μm; $L =$ real	I–V, V_{TH}, V_{BK}
MT50	$W = 50$ μm; $L =$ real	I–V, V_{TH}, V_{BK}
4MT50	$W = 50$ μm; $L =$ real, 4 gates	I–V, V_{TH}, V_{BK}
8MT50	$W = 50$ μm; $L =$ real, 8 gates	I–V, V_{TH}, V_{BK}
MT125	$W = 125$ μm	I–V, V_{TH}, V_{BK}
MT300	$W = 300$ μm	I–V, V_{TH}, V_{BK}
DT1	$W =$ real, 1 gate	I–V, V_{TH}, V_{BK}
DT4	$W =$ real, 4 gates	I–V, V_{TH}, V_{BK}
DT8	$W =$ real, 8 gates	I–V, V_{TH}, V_{BK}
RDT	Real driver	I–V, V_{TH}, V_{BK}
ET	Real ESD	I–V, V_{TH}, V_{BK}
EDT	2 ESDs and driver	I–V, V_{TH}, V_{BK}

LOCOS: local oxidation of silica; W: width; L: length; ESD: electrostatic diode; V_{TH}: threshold voltage; V_{BK}: breakdown voltage.
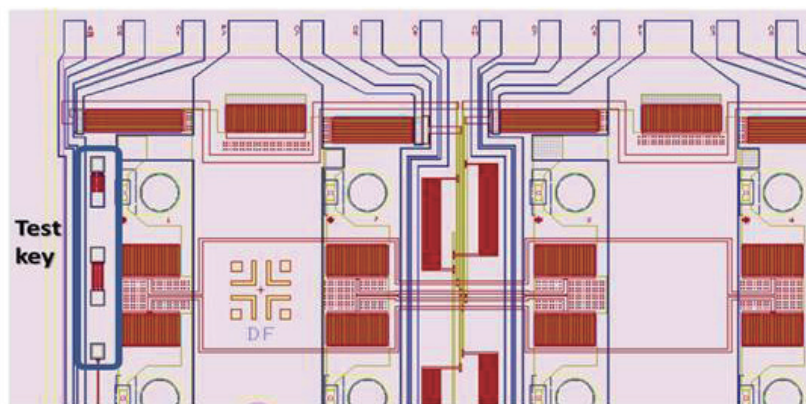

Fig. 1.   (Color online) Test key layout.

Table 2
Nano-inkjet (PCM).

Codename	Content	Eligibility criteria
MMI	Metal_1 to metal_2 insulator	Open, upon LOCOS and poly
MMC	Metal_1 to metal_2 contact	Short
M2O	AlCu etch off	Open
FHO	Flat heater etched off	Open
UHO	Nonflat heater etched off	Open
GMI	Gold to metal_2 isolation	Capacitor leakage
TMI	Tantalum to metal_2 isolation	Capacitor leakage
GMC	Gold to metal_2 contact	—
GGO	Gold to gold etched off	—
FTO	Flat tantalum etched off	—
UTO	Nonflat tantalum etched off	—

LOCOS: local oxidation of silica.

Design rules must be consistent with the actual layout. For example, the minimum line width of poly-Si in the chip is 4 μm, the minimum line spacing is 2.5 μm, and the poly-Si etching off (PPO) of the PCM needs to be the same as the metal to poly isolation (MPI).

Previous processes must be considered together. For example, the heater etched off must be designed with an uneven surface caused by metal_1 and poly-Si in the lower layer; the capacitors of MMI, GMI, and TMI must be set on an uneven surface. For example, GMI must have an uneven surface on the lower layer. On the uneven surface caused by LOCOS, poly, and metal_1, one can test the capacitance of mesh metal_2 and flat metal_3.

2.2 Design of body embedded in source (BES) MOSFET with the base electrode placed in the active area to reduce secondary collapse

The base contact is placed in the active region, located in the source region or adjacent to the source of the BES driving the MOSFET field effect body structure. This structure widely distributes the base contact in the middle of each driving field effect body. This leaves a part of the polysilicon material used for the gate layer in the source region to shield against ion implantation or diffusion of the source drain. This shielding layer is then etched to define the base region, and another type of carrier ion implantation or diffusion is used to make the base electrode. Compared with the traditional structure of placing the base electrode in the field oxide layer, this structure can reduce the field area required by the base electrode. It can also reduce secondary collapse caused by the matrix effect after the MOSFET is turned on, so that the withstand voltage of the field effect body will increase when it is turned on.

The main feature of this structure of the inkjet print head with the drive transistor embedded in the base electrode in the source is that a small part of the source region of the MOS field effect body is vacated at regular intervals for the production of P+ boron dopants. In the base contact, each MOS field effect body can have five to hundreds of base contact points, and they are scattered in each source of the MOS field effect body. The processing method is to use the polysilicon layer of the gate to define the source to prevent N+ diffusion or ion implantation of

the source and drain and then to etch the polysilicon to define the P+ region of the base contact. In the following, we consider three different designs of embedded base-to-source drive MOS field effect body structures as examples with which to compare the current structure.

The manufacturing process is described by entity one as follows.

(a) Silicon oxide and silicon nitride are first used to define the active area of the MOS field effect body on the surface of the silicon substrate, and a thick field oxide layer is grown by LOCOS process oxidation. The thickness of the LOCOS oxide layer is 8000 to 18000 Å.

(b) Silicon nitride and silicon oxide are removed, a gate oxide layer is grown by dry oxygen oxidation, and a polycrystalline silicon layer is then deposited by chemical vapor deposition. Alternatively, only the silicon nitride of the source and drain is removed, the nitride silicon and silicon oxide directly serve as the gate insulating layer, and polysilicon is deposited directly onto the silicon nitride. The gate layer and base shielding layer are defined by lithography and etching. The base shielding layer is located at the source and dispersed in the source area of the field effect body, occupying a part of the area of the source, and is not connected to the polysilicon of the gate. The base shielding layer of this polycrystalline silicon resists phosphorus or arsenic dopants during subsequent N+ diffusion or ion implantation, ensuring that the base of the source region is not implanted with N+ dopants.

(c) Lithography and polysilicon etching are used to define the P+ base region to be doped with boron, and ions are distributed or diffused into the boron dopant.

(d) Chemical vapor deposition is used to deposit silicon oxide and phosphorus-doped silicon oxide of tetraethyl silyl methane or boron-phosphorus-doped silicon oxide as the insulating layer of the MOS field effect body, and a hot melt flow is used to improve the surface (topographic) roundness (smoothness). Then, the gate, drain, and source and base contact holes are defined by lithography and silicon oxide etching. The source and base contact holes can be designed separately, or a shared contact hole design can be adopted. The size of the base contact hole can be smaller than the P+ base area in the *X* direction, or equal to or larger than the P+ base area, but not larger than the polysilicon base shielding area.

(e) The thermal resistance layer and conductive layer are deposited by sputtering or evaporation, the wire and thermal resistance are defined by lithography and etching, and the source and base are connected to the same metal, by connecting to the lowest potential end or the ground.

This structure allows the base to be widely distributed in a driver, and the substrate current does not need to flow long distances to the body contact outside the remote active area, so that the resultant base doping profile value is replaced by the source metal instead of the silicon substrate and is minimized. Another structural entity of the inkjet print head with a driving transistor embedded in the base electrode is mainly used to rely on the source electrode next to the LOCOS area of the field oxide layer. The difference with the entity one is that the position of the polysilicon base shielding layer is across the source and the LOCOS area region, and the P+ base area region is located on the side of the source and is only adjacent to the LOCOS. The base contact hole spans the N+ drain area region and the P+ base area region at the same time and can also only come into contact with the P+ base region.

3. Results

3.1 Specifications of nano-ink

Consumers' purchase of inkjet cartridges is often determined by their impression of print quality and color rendering. Here, the choice of ink cannot be ignored. Furthermore, since the ink fills the entire inkjet cartridge, to determine whether the chemical properties of the ink will affect the life of the internal components of the cartridge and the inkjet efficiency, we need to carefully evaluate the choice of ink. Therefore, basic functional satisfaction and color performance become the specific requirements for ink selection.

In the selection of ink for high-resolution color inkjet heads, there are three main items for judging the suitability of the ink. First, the ink must be compatible with all components that may be in contact with the ink cartridge. In a performance life test, the second item evaluates the impact of ink on inkjet efficiency, and the third item is to judge the print quality of the ink.

The formulation of specifications requires verification of experimental data. In the first compatibility life test of the ink and cartridge components, an environmental testing machine is mainly used for experimental testing. The method of ring testing is to put all the components of the cartridge into the ink container to be tested, and then add the ink. The container is placed in the environmental testing machine, and the cartridge components and ink are regularly observed for abnormal changes in order to record the compatibility life limit of the cartridge components and ink under conditions in the environmental testing machine, and then convert the cartridge components and ink into the normal environment based on experience. The compatible life or the life attenuation value can be measured.

The second item is to evaluate the effect of the ink-ability on inkjet efficiency. The surface tension and viscosity of the ink clearly have direct impacts on the ink drop weight, the diameter of the ink dot, and the diffusion area of the ink drop per unit weight on the paper surface. Some experiments also showed that the surface tension, viscosity, boiling point, volatility, etc. of the ink are directly related to the frequency response of the inkjet and inkjet efficiency. Therefore, the chemistry of the ink has also become an important factor in ink selection.

A study was carried out to analyze the quality of ink printing, including the printed ink dot size, line width, hue, lightness, color degree, water resistance, light resistance, etc. Finally, various inks were printed into patterns to make a questionnaire format, and the acceptabilities of the various inks were compared in a personal subjective way.[10–12]

3.2 Automatic test equipment for component electrical properties

The main purpose of component electrical property testing is to determine whether the MOSFET component can operate normally and to clarify the produced heater characteristics as shown in Fig. 2, so that the layout and manufacturing process can respond to the characteristics. The entire measurement can actually be conducted using the HP4145B DC parameter analyzer for semiconductor components.
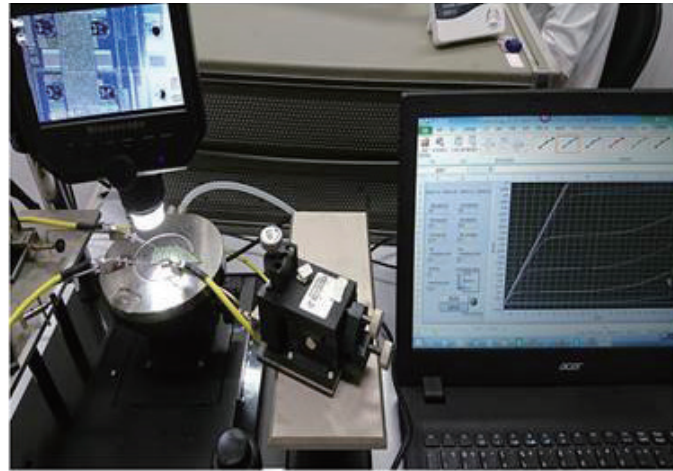
Fig. 2.   (Color online) MOSFET driver measurement.

Another system hardware architecture for electrical measurement is mainly composed of two Keithley Model 2400 source meters, one of which is computerized with a continuous component signal test by a personal computer (PC) through the NI GPIB (National Instruments, General-Purpose Interface Bus) interface; the control program is written in C language. The other one is maintained by the 2400 panel, which is mainly used to change the voltage of the MOS gate. The basic functions of the control program include *I–V* linear test, *I–V* log test, and *V–I* linear sweep. The commonly used function is the *V–I* linear sweep, which is used to measure the drain voltage (V_d) and drain current (I_d) curves from the drain terminal to the source terminal. When the voltage of the gate changes, the entire characteristic curve is completely measured. When measuring the voltage, an enhanced MOSFET is set to a predetermined value. Generally, V_{TH} is set to 10 µA. However, another more common way to measure the critical voltage of a MOSFET is to bias the gate and drain the component at the same potential and then measure its characteristics in the saturation region, because the drain voltage in the saturation region can be expressed as

$$I_D = b(V_{GS} - V_T)^2, \tag{1}$$

where I_D is drain current, b is a constant, V_{GS} is gate to source voltage, and V_T is threshold voltage.

With the straight-line function, V_T and b can be obtained from the intersection of the curve and the horizontal axis. The operation steps of the entire measurement are placing the chip to be tested on an *xyz* stage, adjusting the three probes, and checking whether the contact is good using a microscope. If the object to be tested has been wired to the PC board, it can just be hooked using a hook. The three lines are connected to PS (the upper end of the heater on the drain), A (gate end), and Gnd (source end). The probes come into contact with the input drive signal pads on the chip as shown in Fig. 3. The probes also come into contact with the input drive signal pads on the chip within the entire wafer as shown in Fig. 4.

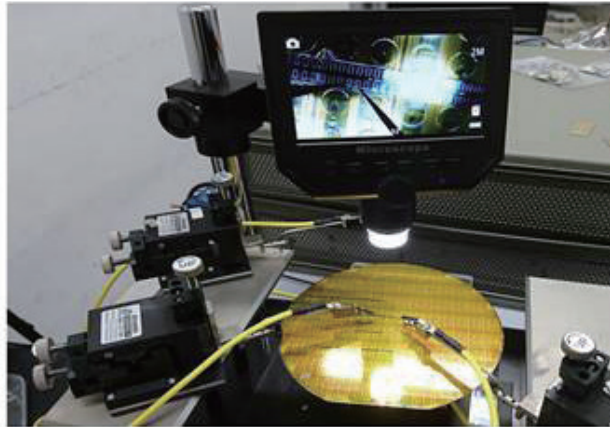Fig. 3.   (Color online) Probes come into contact with the input drive signal pads on the chip.

Fig. 4.   (Color online) Probes come into contact with the input drive signal pads on the chip within the entire wafer.

The grounds of the two Keithley 2400 source meters of the test system are connected together. When starting the measurement, the voltage of the gate is sent out. At this time, one should pay attention to whether the current displayed on the panel of the 2400 instrument is abnormal to determine whether the chip to be tested has leakage. Because the gate terminal of the general MOS has high impedance, the current is very small, but because there is a ground resistance of about 47 kΩ, there will be ten micro-amps of current. The MOSFET threshold voltage is defined as the gate voltage at which significant current begins to flow from the source to the drain (the threshold voltage is 2.3 V), and the *I*–*V* curve is as shown in Fig. 5.

When the MOSFET execution program is run, one follows the computer screen instructions to input the starting voltage, ending voltage, step voltage, and current upper limit in order to begin the measurement. The computer immediately displays the graph of the measurement results after the measurement is completed. After that, one can choose whether to archive the results or not, and then analyze and compare the data using Microsoft® Excel.
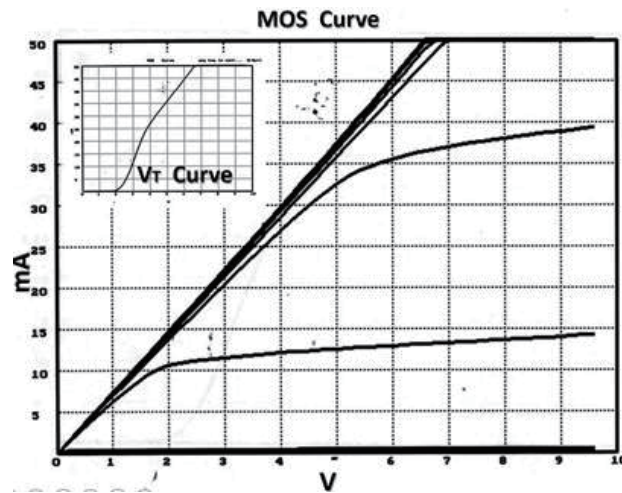
Fig. 5.   Threshold voltage and *I–V* curve.

4.   Discussion

4.1   Low-voltage logic circuit signal measurement results

The purpose of the low-voltage logic circuit design is to determine which nozzle has nano-ink jetting as shown in Fig. 6. Channel 1 of the oscilloscope is the signal processing range of the set 20 groups. Channel 2 is the clock of 20 groups, the purpose of which is to scan the data that needs nano-ink. Channel 3 is the latch data signal of the 20 groups, the purpose of which is to lock the data with nano-ink. Channel 4 is a profile of the nano-ink from the 20 groups.

The oscilloscope measures the signal size of each pad on the chip to determine the sizes of the input buffer, output buffer, and super buffer on the chip circuit to meet the requirements to smoothly push out the load.

4.2   Open pool test of nano-ink

For measuring the open pool of the MOS, one must use the original custom-made drive circuit board and change it to drive the MOS. The connection method is similar to that described above, but because it wants to view the image, the system needs to connect the CCD to the microscope to do that. The strobe's LED is fine-tuned to the proper position to make the image clear. The strobe's light is a strobe light source that must be synchronized to the same frequency as the printing frame. As long as a good MOS and heater can be found, it can see the bubbles on the heater from the image guided by the CCD to the screen as shown in Fig. 7. As for the resistance measurement on the cassette, the Keithley 7001 switching system and two Keithley 400 instruments are used for the voltage source and resistance measurements. With appropriate software, all resistance values can be quickly measured.

After the chip of the nano-ink jet printer head for optoelectronic applications is completed, the open pool test of nano-ink is conducted. After the entire film process is completed and
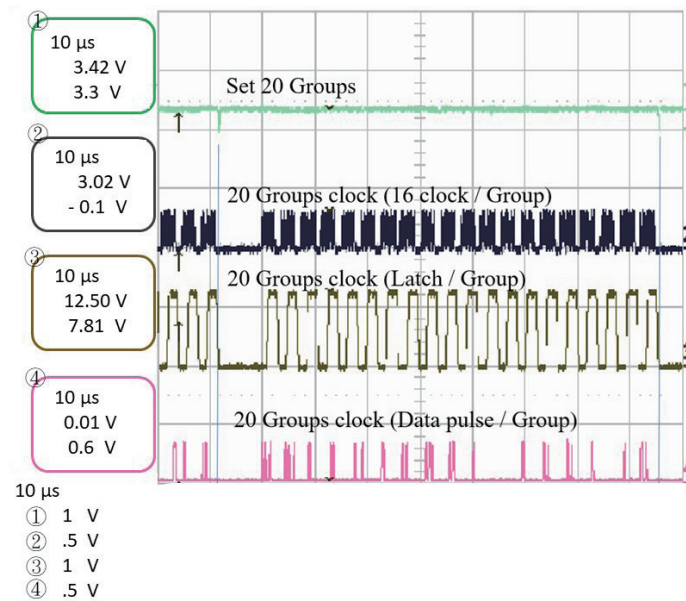
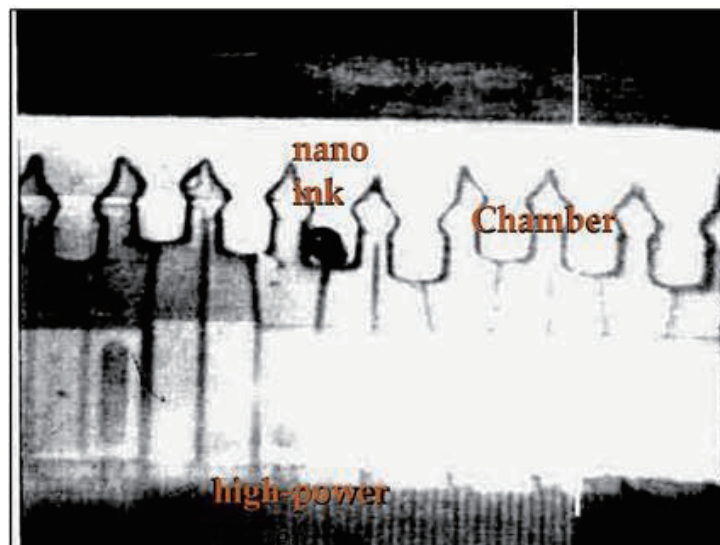Fig. 6.   (Color online) The oscilloscope measures the signal formation.

Fig. 7.   (Color online) Bubble growth distribution chart.

before the nozzle sheet is pressed, an ink channel and ink tank are formed by a layer of dry film of about 30 μm thickness above the heater of the inkjet head. Therefore, if energy is supplied to the heater, the ink is injected, and the growth and decline of bubbles occurs. To facilitate observation, pure water is used instead of ink. Since pure water is transparent, the growth and decline of hot bubbles on the heater surface can be directly observed from the top of the inkjet head. Before the chip open pool test, according to the previously measured MOS circuit characteristics, PS11, G11, and A4 were randomly selected as the groups paired with the probes,

and a 10 V, 2.5 μs pulse width at 9.8 kHz was added to the gate driver of the MOS. It was found that the heater corresponding to the paired group produced the phenomenon of bubble growth and decline, the starting voltage was calculated to be 11 V, and the lifespan was 1.2×10^7 times. However, the voltage of the drain and source of the machine was 11.4 V, and the measured gate voltage was 10.6 V. Therefore, the current chip starting voltage was still too high and had to be lowered so that the voltage working range was not too narrow.

4.3 DNA droplet inkjet printing

The DNA droplet ejection that addresses the same time period drive (Fig. 8), with a next-generation single-stone high-level DNA spray system, includes integrated logic multiplexing, a liquid spray MEMS structure, a high-voltage ESD protection circuit system, and optimization for research and development. For research and development in the field of DNA detection and medical electronics, the developed DNA spray array is quantitatively distributed on the glass slide, and the system signal is designed using logical multiplexing technology to achieve DNA sequencing combinations and nucleotide sequencing. Molecules use different methodologies to control chemical reactions in sequence, forming nucleic acid sequences one by one, and quickly producing precise (accurate positioning and uniform orientation) and ultrahigh-density (1×10^6–2×10^6 dots) wafers. There are two main synthesis methods. One is to use liquid jet technology to spray nucleotides like ink into specific positions for solid-phase phosphoramidite chemistry. The other one is photolithography, which uses a photomask to control the reaction and a photochemical reaction for synthesis.
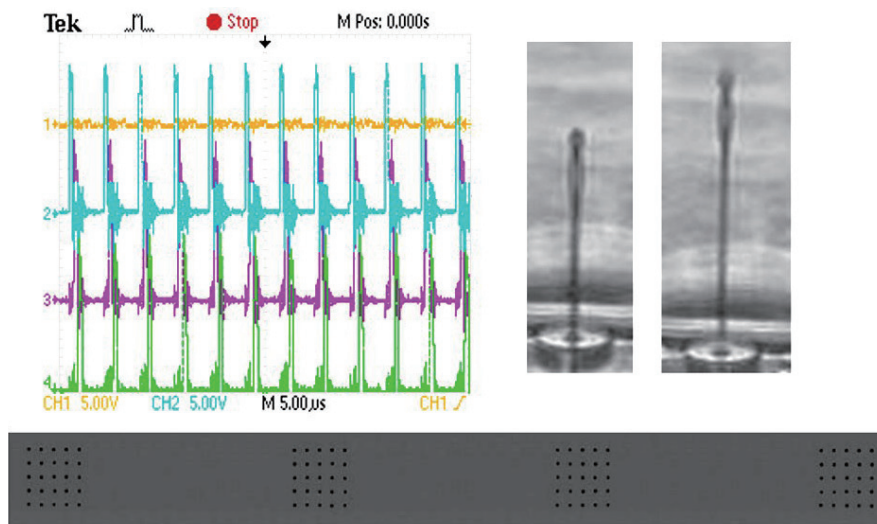

Fig. 8.   (Color online) DNA droplet ejection that addresses the same time period drive.

5.   Conclusions

The technological development of an integrated nano-inkjet chip circuit design architecture of a multiplexer can include a nano-ink inkjet unit cell. The structure or composition of this research concept was to control more than 1296 heaters. This chip system includes a low-voltage logic circuit design, high-voltage and high-power drive components, and a micro-electromechanical nano-inkjet structure on one chip. The application of nano-ink is more effective than that of ordinary inks in the field of optoelectronics. Digital logic circuits, optoelectronic thin film technology, and micro-electromechanical technology are all integrated on a single chip. The entire chip is a very large digital logic circuit that controls more than 1000 nano-ink nozzles. It also deploys nano-ink droplets by integrating the nano-ink jet chip. It can be seen from this architecture that inkjet printing technology is rapidly updated. DNA spray arrays can be quantitatively distributed on a glass slide. With the advantage of low price, nano-ink inkjet printing has the same printing speed and quality as industrial applications.

Acknowledgments

References

1   J. C. Liou, C. W. Peng, P. Basset, and Z. X. Chen: Micromachines **12** (2021) 1. https://doi.org/10.3390/mi12010025

2   F. G. Tseng, C. J. Kim, and C. M. Ho: J. Microelectromech. Syst. **11** (2002) 437. https://doi.org/10.1109/JMEMS.2002.802900

3   J. C. Liou, C. H. Liu, and C. J. Chen: 2004 IEEE/SEMI Advanced Semiconductor Manufacturing Conf. and Workshop (IEEE, 2004) 413–419. https://doi.org/10.1109/ASMC.2004.1309607

4   J. C. Liou, T. J. Su, W. J. Wen, and W. C. Lin: 2016 Int. Conf. Advanced Materials for Science and Engineering (IEEE, 2016). https://doi.org/10.1109/ICAMSE.2016.7840211

5   J. C. Liou and W. D. Lin: 3rd Int. Conf. Green Technology and Sustainable Development (IEEE, 2016) 82–85. https://doi.org/10.1109/GTSD.2016.29

6   U. Kessararat, P. Tawee, M. Thitima, W. Anurat, and T. Adisorn: 4th 2011 Biomedical Engineering Int. Conf. (IEEE, 2012) 207–211. https://doi.org/10.1109/BMEiCon.2012.6172053

7   F. G. Tseng, C. J. Kim, and C. M. Ho: J. Microelectromech. Syst. **11** (2002) 427. https://doi.org/10.1109/JMEMS.2002.802900

8   J. C. Liou and F. G. Tseng: DTIP 25 (2007). https://doi.org/10.48550/arXiv.0802.3079

9   C. LaMont, J. Aditya, A. Vargas-Garcia Cesar, J. P. Michael, and Z. Ryan: IEEE 56th Annu. Conf. Decision and Control (IEEE, 2017) 4106–4111. https://doi.org/10.1109/CDC.2017.8264262

10 S. J. Shin, K. Kuk, J. W. Shin, C. S. Lee, Y. S. Oh, and S. O. Park: TRANSDUCERS '03. 12th Int. Conf. Solid-State Sensors, Actuators and Microsystems. Digest of Technical Papers (IEEE, 2003) 380–383. https://doi.org/10.1109/SENSOR.2003.1215333

11 R. Nayve, M. Fujii, A. Fukugawa, T. Takeuchi, M. Murata, Y. Yamada, and M. Koyanagi: J. Microelectromech. Syst. **13** (2004) 814. https://doi.org/10.1109/MEMSYS.2003.1189785

12 W. R. Matthew, M. J. Nan, and B. F. Richard: IEEE Sens. J. **13** (2013) 4733. https://doi.org/10.1109/JSEN.2013.2273828

13   J. H. Park and Y. S. Oh: Microsyst. Technol. **11** (2005) 16. https://doi.org/10.1007/s00542-004-0431-2

14   S. K. Sarkar, H. Gupta, and D. Gupta: IEEE Trans. Nanotechnol. **16** (2017) 375. https://doi.org/10.1109/TNANO.2017.2658341

15   T. Lindemann, H. Ashauer, T. Goettsche, H. Sandmaier, Y. Yu, R.P. Peters, D. Sassano, A. Bellone, A. Scardovi, R. Zengerle, and P. Koltay: 18th IEEE Int. Conf. Micro Electro Mechanical Systems (IEEE, 2005) 560–563. https://doi.org/10.1109/MEMSYS.2005.1453991

16   J. C. Liou and C. F. Yang: Microelectron. Reliab. **91** (2018) 243. https://doi.org/10.1016/j.microrel.2018.10.012

17   U. Kessararat, P. Tawee, M. Thitima, W. Anurat, and T. Adisorn: 4th 2011 Biomedical Engineering Int. Conf. (IEEE, 2012) 207–211. https://doi.org/10.1109/BMEiCon.2012.6172053

18   A. Ashkin and J. M. Dziedzic: Appl. Optics **20** (1981) 1803. https://doi.org/10.1364/AO.20.001803

19   H. B. Lin, A. L. Huston, B. L. Justus, and A. J. Campillo: Opt. Lett. **11** (1986) 614. https://doi.org/10.1364/ol.11.000614

20   J. Y. Lee, H. C. Park, J. Y. Jung, and H. Y. Kwak: J. Heat Transfer. **121** (2003) 687. https://doi.org/10.1115/1.1571844

21   S. C. Hill, D. H. Leach, and R. K. Chang: J. Opt. Soc. Am. B **10** (1993) 16. https://doi.org/10.1364/JOSAB.10.000016

22   T. M. Eggenhuisen, Y. Galagan, A. Biezemans, M. Coenen, J.Gilot, P. Groen, and R. Andriessen: 2014 IEEE 40th Photovoltaic Specialist Conf. (IEEE, 2014) 1–4. https://doi.org/10.1109/PVSC.2014.6925523

23   T. Lindemann, H. Ashauer, Y. Yu, D. S. Sassano, R. Zengerle, and P. Koltay: J. Microelectromech. Syst. **16** (2007) 420. https://doi.org/10.1109/JMEMS.2007.892796

24   M. Einat and M. Grajower: J. Microelectromech. Syst. **19** (2010) 391. https://doi.org/10.1109/JMEMS.2010.2040946

25   S. J. Shin, K. Kuk, J. W. Shin, C. S. Lee, Y. S. Oh, and S. O. Park: Sens. Actuators, A **114** (2004) 387. https://doi.org/10.1016/j.sna.2003.11.030.